TOWARDS A LOW IMPEDANCE VACUUM SYSTEM FOR THE FCC-ee

P. Krkotić *, M. Ady, V. Baglin, P. Chiggiato, C. Garion, V. Giovinco,
G. de Gois Saretti, M. Morrone, CERN, 1217 Geneva, Switzerland

Abstract

The design of the Future electron–positron Circular Collider (FCC-ee) vacuum system integrates vacuum engineering, impedance mitigation, and surface functionalisation to achieve compatibility with high beam currents and sustained operational stability. Based on these design principles, this contribution presents an overview of the principal vacuum components and outlines the studies conducted to evaluate and optimise their electromagnetic and vacuum performance. Particular emphasis is placed on the interplay between material properties, surface treatments, and component geometry, as well as on the distribution and integration of vacuum elements and transitions within the accelerator. Impedance studies were performed to evaluate the electromagnetic impact of representative vacuum components. The main findings are summarised, highlighting the achieved performance and outlining directions for further optimisation.

INTRODUCTION

The FCC-ee is a proposed high-luminosity lepton collider operating in the energy range from the Z pole (45.6 GeV) to the $\bar{t}t$ threshold (182.5 GeV) [1]. High beam currents up to 1.2 A, short bunch lengths of 2–15 mm, and intense synchrotron radiation (SR) power (45 MW/beam) impose stringent constraints on the vacuum system, particularly with regard to beam-coupling impedance and trapped electromagnetic (EM) fields that can limit beam stability and generate significant parasitic power deposition.

The adoption of the local chromatic correction (LCC) optics scheme [2, 3] introduces a novel arc-cell structure shown in Fig. 1, defining the vacuum component integration strategy. In this configuration, each arc half-cell consists of a periodic sequence of sextupole and quadrupole magnets (or vice versa) together with a beam position monitor installed on girders, followed by three dipole magnets. The arc sections account for approximately 77 % of the collider circumference (~70 km of vacuum system). At this scale, even small impedance contributions from individual components can accumulate to a significant fraction of the machine impedance budget, making impedance reduction a central design requirement.

The FCC-ee vacuum system is based on an integrated design approach, in which vacuum, thermal, mechanical, and impedance-related constraints are considered simultaneously from the earliest design stage. Material selection, surface treatment, and component geometry are optimised alongside impedance-aware assembly solutions to minimise both broadband and narrowband contributions. Particular attention is devoted to identifying and mitigating resonances and radio-frequency (RF) discontinuities.

In this paper, the dominant impedance sources of the principal vacuum elements are analysed together with optimisation guidelines for their design.

FCC-EE ARC VACUUM COMPONENTS

Vacuum Chamber

The vacuum chamber (VC) constitutes a dominant broadband impedance source through the resistive wall impedance (RWI), arising from the finite surface impedance of the chamber material, coating, and surface finish, and scaling linearly with the machine length.

The baseline VC section shown in Fig. 2 consists of an extruded oxygen-free silver-bearing (OFS) copper (≥99 % IACS[1]) profile, coated with a 150-200 nm thick non-evaporable getter (NEG) layer. The horizontally symmetric antechamber geometry separates the 60 mm diameter beam aperture from the SR fan, while providing space for localised SR absorbers and preserving a nearly circular cross-section to minimise geometric impedance contributions.

The NEG coating provides distributed pumping and reduces photon-stimulated desorption and secondary electron yield [4, 5]. Its thickness is optimised to minimise the additional RWI contribution while maintaining adequate vacuum performance and acceptable single-bunch instability thresholds [6, 7]. In this thin-film regime, the RWI is dominated by the coating thickness and remains predominantly inductive, as shown in Fig. 3, where the dashed green curve indicates the increase in surface reactance relative to smooth copper.

Surface roughness also contributes to the impedance due to the broad beam-frequency spectrum extending to tens of GHz and the resulting small skin depths. Using the multi-

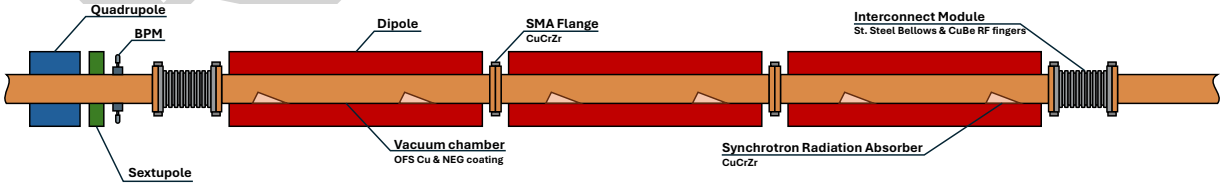

Figure 1: Schematic of a representative arc cell configuration for the FCC-ee LCC optics layout.

* patrick.krkotic@cern.ch

[1] IACS: conductivity relative to annealed pure copper (100%).

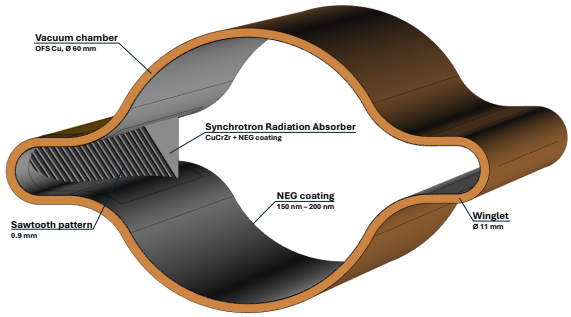

Figure 2: FCC-ee vacuum chamber including localised synchrotron radiation absorber.

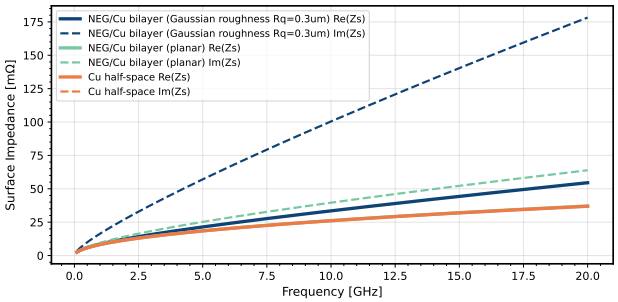

Figure 3: Surface impedance comparison between copper and 175 nm NEG-coated smooth and rough surfaces. In the smooth-surface case, the real and imaginary parts coincide for bare copper (orange curves). For NEG-coated copper in the smooth-surface case, the real part (turquoise line) overlaps with the bare copper curve and is thus not visible.

layer gradient model [8], even with a Gaussian-distributed rms roughness of $R_q = 0.3\,\mu\text{m}$, both the real and imaginary parts of the surface impedance increase relative to smooth copper, see Fig. 3. The additional effect of the NEG coating on a rough surface remains predominantly inductive. The enhanced real component results in beam-induced power dissipation of 14 W/m during Z-mode operation, evaluated using BIHC [9], while the roughness contribution to the imaginary component exceeds the inductive contribution of the NEG coating in the smooth consideration and may further reduce beam-stability margins, something which is still under evaluation. Impedance mitigation therefore requires both controlling the NEG coating thickness and limiting the VC surface roughness, potentially through dedicated surface treatment prior to or during coating deposition.

Synchrotron Radiation Absorber

Localised SR absorbers are installed in the outer winglets of the dipole VCs (Fig. 2) to intercept photons and shield downstream components [10]. Since they introduce geometric discontinuities, the design requires smooth transitions and careful placement within the winglets. Photon-tracking simulations using SYNRAD [11], combined with studies of beam-induced current paths, were used to balance photon reflection into the VC while limiting wakefield excitations.

The current design uses 39 cm-long copper-chromium-zirconium (CuCrZr, 80 % IACS) absorbers, NEG-coated and

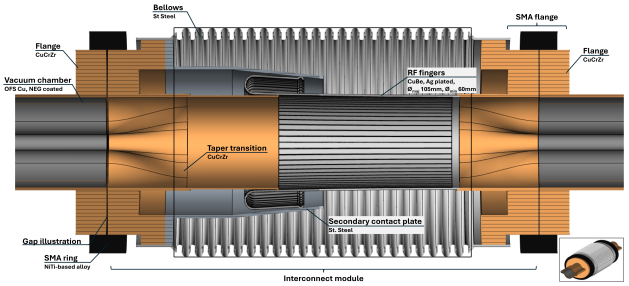

Figure 4: FCC-ee interconnect module with SMA flanges at both ends. A potential transition gap is visualised.

laser-welded to the VC at approximately 5.4 m intervals. The trapezoidal geometry features a photon-intercepting surface inclined by 45° to the beam axis and tilted transversely by 6° to distribute SR power while satisfying thermomechanical constraints. A sawtooth pattern with 0.9 mm step height on the intercepting surface is aligned with the beam-induced current flow to minimise its additional impedance contribution by avoiding transverse step crossings. Protrusion of the absorber into the VC is (and must be) avoided; thus, the absorbers are recessed by 3.25 mm into the winglet relative to the round chamber boundary. The weld geometry is positioned away from regions of maximum surface current density to minimise its impact.

Numerical studies show that the longitudinal impedance is predominantly inductive, with a minor resistive component due to the exposed absorber surface area. Weak resonances are nevertheless observed near the cut-off frequencies of propagating waveguide modes, indicating residual EM coupling that remains under investigation. The corresponding beam-induced power deposition is about 1 W per absorber during Z-pole operation, negligible compared with the expected SR power load of about 3.5 kW per absorber. Unfortunately, the transverse impedance could not be resolved within the numerical accuracy of the present simulations.

Shape Memory Alloy Flanges

The shape memory alloy (SMA) flange design (Fig. 4) features an elliptic CuCrZr aperture (122 mm × 145 mm). Vacuum sealing is achieved using a copper gasket compressed laterally by a thermally activated SMA ring [12], enabling, in principle, a zero-length transition that preserves VC geometry continuity across the interface.

Mechanical simulations nevertheless predict that, in combination with CuCrZr, the SMA compression forces may produce small gaps between adjacent flange surfaces. These cavity-like volumes may support low-frequency resonances coupled to beam harmonics, increasing local power deposition and flange temperature, which, based on coupled EM and thermomechanical analyses, must remain below approximately 180°C, corresponding to about 240 W of beam-induced power.

If the resonances remain sufficiently detuned from the beam harmonics, gaps of up to about 0.5 mm remain acceptable below the aforementioned threshold. However, under

Table 1: FCC-ee arc vacuum component counts for one beam, based on the LCC optics layout (V106.2.2) [13].

Component	Total Number	Power [MW]
Vacuum chamber	8 760	0.96
SR absorber	13 152	0.01
Flange (0.2 mm gap)	13 152	1.91
Interconnect module	4 384	1.34

conservative worst-case resonance and beam-harmonic overlap assumptions, the allowable gap width reduces to 0.2 mm corresponding to approximately 200 W of deposited power during Z-pole operation.

Interconnect Modules

Interconnect modules (IMs), incorporating bellows shielded by RF fingers, maintain RF continuity between adjacent VCs while accommodating bake-out expansion, assembly tolerances, and alignment offsets. In the FCC-ee, the LCC optics configuration requires up to 80 mm longitudinal compression and 5 mm transverse misalignment during bake-out, leading to the RF-shielding concept shown in Fig. 4.

The assembly consists of tapered transitions from the VC to an oval bellows geometry whose minor and major axes correspond to the total VC height and width, including the winglets, while minimising taper angles over a short distance. RF shielding consists of straight RF fingers, ensuring continuous image-current paths while suppressing EM-field coupling into the outer bellows volume. A looped double-contact configuration is envisaged for electrical reliability and shielding stability. Since degraded RF contact quality may significantly increase impedance and local beam-induced heating [14], low and stable contact resistance remains essential. Copper beryllium (CuBe), with silver plating, is hence selected for the RF fingers due to its favourable electrical and mechanical properties [15, 16].

Complete suppression of EM coupling to the outer bellows volume is not achievable, even with ideal RF contacts, due to the finite gaps required between adjacent RF fingers. The coupling strength, however, can be controlled through the gap geometry, particularly the ratio of RF-finger to gap area and the RF-finger thickness, currently about 0.5 mm, 11 cm, and 1 mm for the finger spacing, length, and thickness, respectively. The design therefore aims to minimise coupling to the outer bellows volume and to reduce the bellows volume itself, shifting resonances towards higher frequencies and thereby reducing their interaction with the beam spectrum.

In the FCC-ee, however, attention must also be paid to the inner IM volume, since the enlarged oval cross-section locally lowers the cut-off frequency relative to the nominal VC and may favour trapped-field formation within the module, with beam-induced power deposition reaching up to 300 W during Z pole operation. The tapers, therefore, require dedicated studies to guide the IM design and suppress power propagation into the module and surrounding equipment.

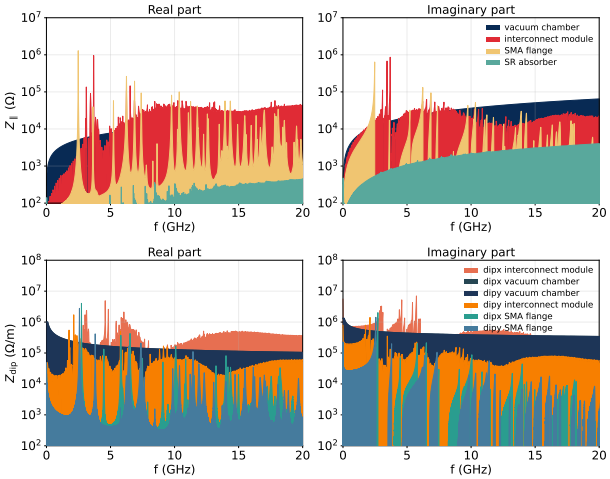

Figure 5: Preliminary integrated FCC-ee arc vacuum system impedance: longitudinal (top), transverse dipolar (bottom).

ARC IMPEDANCE CONTRIBUTION

The integrated arc impedance shown in Fig. 5 is broadband and dominated by the distributed RWI of the OFS Cu VC, with surface roughness providing an additional contribution. Since no room-temperature material with higher electrical conductivity is currently available, further reduction of the RWI mainly requires increasing the VC diameter. The local geometric contributions from the SR absorbers remain comparatively small, indicating favourable integration of the absorber within the VC geometry.

In contrast, narrow-band resonances due to residual RF discontinuities, e.g. flange gaps, may contribute significantly to the impedance spectrum at certain resonance frequencies and result in strong local beam-induced heating. The dipolar impedance spectra additionally show resonance shifts for oval components, such as the SMA flanges, in both transverse planes, reflecting the effect of non-circular local geometries on the impedance response. The total beam-induced power dissipated in the arc vacuum system is approximately 4.3 MW per beam, with the individual component contributions summarised in Table 1. This power loss must be compensated for by the RF system.

CONCLUSION

We have briefly outlined the current status of the FCC-ee arc vacuum system design for the latest LCC optics layout, focusing on the associated impedance constraints and their impact on component design. Extensive numerical and analytical studies remain ongoing and will be complemented by prototype production and electromagnetic test-bench measurements. The studies must additionally be extended to cover all four FCC-ee energy regimes.

ACKNOWLEDGEMENTS

We thank the FCC-ee Impedance team, in particular C. Antuono, M. Migliorati, and C. Zannini, as well as S. Calatroni, for the fruitful discussions contributing to this work.

REFERENCES

[1] M. Benedikt *et al.*, "Future circular collider feasibility study report - Volume 2: Accelerators, technical infrastructure and safety", *Eur. Phys. J. Spec. Top.*, vol. 234, pp. 5713–6197, 2025. doi:10.1140/epjs/s11734-025-01967-4

[2] G. Roy *et al.*, "FCC-ee optics comparison report", Dec. 2025.

[3] P. Raimondi *et al.*, "Local chromatic correction optics for future circular collider e^+e^-", *Phys. Rev. Accel. Beams*, vol. 28, no. 2, p. 021002, Feb. 2025. doi:10.1103/PhysRevAccelBeams.28.021002

[4] R. Kersevan, "Vacuum system of the FCC-ee", in *Proc. eeFACT'22*, Frascati, Italy, pp. 244–246, Feb. 2022. doi:10.18429/JACoW-eeFACT2022-THXAS0104

[5] F. Yaman *et al.*, "Mitigation of electron cloud effects in the FCC-ee collider", *EPJ Tech. Instrum.*, vol. 9, no. 1, p. 9, Aug. 2022. doi:10.1140/epjti/s40485-022-00085-y

[6] E. Belli *et al.*, "Electron cloud buildup and impedance effects on beam dynamics in the Future Circular e^+e^- collider and experimental characterization of thin TiZrV vacuum chamber coatings", *Phys. Rev. Accel. Beams*, vol. 21, no. 11, p. 111002, Nov. 2018. doi:10.1103/PhysRevAccelBeams.21.111002

[7] M. Migliorati *et al.*, "Impedance modelling and collective effects in the future circular e^+e^- collider with 4 IPs", *EPJ Tech. Instrum.*, vol. 9, p. 10, 2022. doi:10.1140/epjti/s40485-022-00084-z

[8] G. Gold and K. Helmreich, "Modeling of transmission lines with multiple coated conductors", in *46th EuMC*, pp. 635–638, 2016. doi:10.1109/EuMC.2016.7824423

[9] L. Sito, F. Giordano, G. Rumolo, B. Salvant, C. Zannini, and E. de la Fuente, "A Python package to compute beam-induced heating in particle accelerators and applications", in *Proc. of HB'23*, Geneva, Switzerland, Oct. 2023, pp. 611–614. doi:10.18429/JACoW-HB2023-THBP52

[10] M. Morrone, C. Garion, R. Kersevan, S. Rorison, and P. Chiggiato, "Preliminary design of the FCC-ee vacuum chamber absorbers", *J. Phys. Conf. Ser.*, vol. 2687, no. 2, p. 022011, Jan. 2024. doi:10.1088/1742-6596/2687/2/022011

[11] R. Kersevan and M. Ady, "Recent developments of Monte-Carlo codes Molflow+ and Synrad+", in *Proc. IPAC'19*, Melbourne, Australia, pp. 1327–1330, Jun. 2019. doi:doi:10.18429/JACoW-IPAC2019-TUPMP037

[12] F. Niccoli, V. Giovinco, C. Garion, C. Maletta, and P. Chiggiato, "NiTi shape memory alloy pipe couplers for ultra-high vacuum systems: development and implementation", *Smart Mater. Struct.*, vol. 31, no. 6, p. 065014, May 2022. doi:10.1088/1361-665X/ac6999

[13] FCC ee model repository, 2026, https://gitlab.cern.ch/acc-models/fcc/acc-models-fcc-ee/-/releases/LCC_106.2.2

[14] C. Antuono *et al.*, "Impact of high-intensity LHC beam operation on warm vacuum modules", *Phys. Rev. Accel. Beams*, vol. 28, no. 4, p. 041001, Apr. 2025. doi:10.1103/PhysRevAccelBeams.28.041001

[15] E. Metral *et al.*, "Lessons learned and mitigation measures for the CERN LHC equipment with RF fingers", in *Proc. IPAC'13*, Shanghai, China, May 2013, paper TUPWA042, pp. 1802–1804. https://jacow.org/IPAC2013/papers/TUPWA042.pdf

[16] S. Calatroni *et al.*, "Design aspects of the RF contacts for the LHC beam vacuum Interconnects", 2001. https://cds.cern.ch/record/514353